The dynamics of a double-cell hydrothermal system in triggering seismicity at Somma-Vesuvius: results from a high-resolution radon survey (revisited)

UNIVERSITÀ DEGLI STUDI DI TORINO

Cigolini C. (2010) The dynamics of a double-cell hydrothermal system in triggering seismicity at Somma-Vesuvius: results from a high-resolution radon survey (revisited). Bull. Volcanology, 72, 693-704, doi: 10.1007/s00445-010-0355-x

The dynamics of a double-cell hydrothermal system in triggering seismicity at Somma-Vesuvius: results from a high-resolution radon survey (revisited)

Corrado Cigolini

Dipartimento di Scienze Mineralogiche e Petrologiche
Università degli Studi di Torino
Via Valperga Caluso 35
10125 Torino, Italy.

e-mail: corrado.cigolini@unito.it
FAX: +39-011-6705128

Key words: Radon, hydrothermal system, cyclic seismicity, rock-permeability, porosity

Abstract

The data collected at Somma-Vesuvius during the 1998-1999 radon surveys have been revisited and reinterpreted in light of recent geophysical and geochemical data. The duration of selected radon anomalies, together with the decay properties of radon, have been used to estimate the permeability and porosity of rocks of the deep hydrothermal system. The current local cyclic seismicity is explained by means of a double convective-cells model. Convective cells are separated by a low permeability horizon located at about 2-2.5 km below sea level. Fluids convecting within the upper cells show temperatures ranging 300-350 °C. Rock permeabilities in this sector are estimated in the order of 10^{-12} m^2, for porosities (ϕ) of about 10^{-5} typical of a brittle environment where fluid velocities may reach ~800 m/day. Fluid temperatures within the lower cells may be as high as 400-450 °C, being consistent with supercritical regimes. The hydrodynamic parameters for these cells are lower, with permeability $k \sim 10^{-15}$ m^2, and porosity ranging 10^{-6} - 10^{-7}. Here, fluid motion toward the surface is ruled by the fracture network within a porous medium approaching a brittle-ductile behaviour, and fluid velocities may reach ~1800 m/day. The low permeability horizon is a layer where upper an lower convecting cells converge. In this region, fluids (convecting both at upper and lower levels) percolate through the wallrock and release their brines. Due to self-sealing processes, permeability within this horizon reaches the critical values to keep the fluid pressure near the lithostatic pressure (for $k \sim 10^{-18}$ m^2). Deep fluid pressure build ups precede the onset of hydrothermally-induced earthquakes. Permeability distribution and rocks' strength do not exclude that the next eruption at Somma-Vesuvius could be preceded by a seismic crisis eventually leading to a precursory phreatic explosion. The coupling of these mechanisms has the potential of inducing pervasive failure within rocks of the hydrothermal shell, and may be a prelude to a magmatic eruption. It is finally emphasised that the integrated analysis of seismic and geochemical data, including radon emissions, could be successfully used in testing temperature distributions and variations of porosity and permeability in active geothermal reservoirs.

Introduction

The cone of Mount Vesuvius (1281 m above sea level) has grown within the Somma Caldera which was affected by major collapses between 18 ka and the 79 A.D. plinian eruption. High-resolution seismic tomography (Zollo et al., 1998), indicate the existence of a very low-velocity zone at a depth of about 10-12 km below Mount Vesuvius. This discontinuity is likely to represent the top of a sill-like reservoir (Auger et al., 2001; De Natale et al., 2006). This reservoir is surrounded by a thermometamorphic-metasomatic shell that partially affects

limestones and dolomites of the Miocene basement rocks. Fragments of these materials have been periodically ejected during Vesuvian eruptions (Barberi and Leoni, 1980; Belkin et al. 1995; Del Moro et al., 2001).

Local seismicity is concentrated below the caldera and it is characterised by cyclic swarm sequences (about 200 events/year with duration magnitude $0.4 \leq M_D \leq 3.6$). Hypocenters may be as deep as 6 km below sea level (b.s.l.), with most of the "foci" clustering at a depth of 2-3.5 km b.s.l. (Cassano and La Torre, 1987; Ventura and Vilardo, 1999a). The M_D 3.6 earthquake of 9 October 1999, with a hypocentral depth of 3 km below the top of Mount Vesuvius (the largest in the catalog of INGV Vesuvian earthquakes), has been ascribed to cracking and/or fluid flow within the deep hydrothermal system (Pandolfi et al., 2006). According to Zollo et al. (2002) there was no significant departure from a pure shear double-couple mechanism during the onset of this event, thus suggesting a tectonic-like fracture mechanism. This view has been challenged by De Natale et al. (2004) who suggested that larger Vesuvian earthquakes can be interpreted as a result of a volumetric expansion likely related to fluid transfer.

The relationships between regional earthquakes and eruptions have been investigated by Nostro et al. (1998) who found that eruptive events are generally preceded (less than a decade) by earthquakes on the Appenine chain normal faults. Conversely, eruptions at Vesuvius seem to have weaker effects on Appenine earthquakes. Borgia et al. (2005) have shown that Somma-Vesuvius has been spreading onto its sedimentary substratum since 3,600 years and this process is currently active. The deep structure of Somma-Vesuvius has been recently investigated by integrating seimic and gravimetric data (Tondi and De Franco, 2003) and by refined electromagnetic techniques (Di Maio et al., 1998; Müeller et al., 1999). In particular, the latter authors suggested the existence of a low resistivity layer (from 1 to 5 km b.s.l.), likely generated by the aqueous fluids of the hydrothermal system.

Recently, Chiodini and Marini (1998) and Chiodini et al. (2001) showed that deep fluids are in equilibrium with NaCl brines at temperatures of 360-450 °C . Federico et al. (2004) constructed a model for goundwaters' circulation in this sector of the Campanian region considering the magma-derived gas influx within the local acquifer. Cigolini et al. (2001) analysed radon emissions within the summit area of Somma-Vesuvius and discriminated volcanically-related earthquakes from regional seismic events. In addition, by utilizing the decay properties of ^{222}Rn, they gave preliminary estimates of the hydraulic parameters of the hydrothermal system.

Radon, essentially represented by the isotope ^{222}Rn (with a half life of 3.82 days), is a radioactive gas produced from the decay of uranium bearing rocks and has been successfully used to track degassing along active faults (Burton et al., 2004) and flanks of open-conduit

volcanoes (Cigolini et al., 2005). Furthermore, its spatial and temporal variations have been regarded as precursors of earthquakes (e.g., Fleischer and Mogro-Campero, 1985; Igarashi et al., 1995; Planicić et al., 2004) and variations in volcanic activity (Cox, 1980; Thomas et al., 1986; Connors et al., 1996), including major paroxysmal eruptions (Chirkov, 1975; Cigolini et al., 2005) as well as earthquake-volcano interactions (Cigolini et al., 2007).

Here, I further discuss the data collected during our previous high resolution radon surveys at Somma-Vesuvius (Cigolini et al., 2001) and revisit them in light of the geochemical models of Chiodini et al. (2001) on deep high temperature fluids. I will then propose a *double-convective cell* model for the deep hydrothermal system and analyse the role of hydrothermal dynamics in modulating Vesuvian cyclic seismicity. It is finally suggested that these processes may eventually lead to phreatic eruptions that, in turn, could prelude the onset of magmatic eruptions.

Radon Monitoring at Somma-Vesuvius

The network for the 1998-1999 radon survey has been deployed by taking into account the summit structures of Somma-Vesuvius. These were mapped on the basis of field observations and photogeological studies (cf., Cigolini et al., 2001). They consist of a system of faults and fractures striking NW-SE and NNE-SSW that reflect deeper tectonic features (Bianco et al., 1998) reactivated during recent eruptions (namely 1794, 1906 and 1944). These structures are located within the Somma Caldera. Subsequent local adjustments have been controlled by this conjugate system of faults whose reactivation seem to post-date a moderate collapse that occurred along the western side of the volcano. Sampling stations were deployed along these major structural features (Fig. 1b). Data were collected for stations located on the NNE-SSW fault, the NW-SE fault, the caldera edge and bottom.

Soil radon measurements were acquired with charcoal canisters (Prati et al., 1992) and track-etch detectors (cf., Bonetti et al., 1991). Both were placed in subsurface pipe-like samplers (1 m long with a diameter of 12 cm, which were set to a depth of about 60 cm) isolated by a cap to minimize condensation and to keep humidity as constant as possible. The use of charcoal canisters (Cigolini et al., 2001) has the advantage of minimising the exposure time to 2-4 days, thus increasing the possibility of correlating radon emissions with local and regional seismicity. ^{222}Rn background values in the surrounding region were measured at distances of about 6 to 18 km from the Vesuvius cone (at Ercolano and Nocera Inferiore) and range between 0.02 and 0.1 Bq/lt. Data have been collected on soils of the sampling sites (0.22-0.43 Bq/kg; see Cigolini et al., 2001; Figure 3) and exclude anomalous radon emissions due to the presence of radioactive minerals.

FIG. 1

Two major seismic regional events were recorded by our network during the 1998-1999 survey (Fig. 1). The first, was the M_w=5.4 earthquake of 18 May, 1998 with epicentre in the Tyrrhenian Sea (INGV catalog at http://www.ingv.it/CSI/ and Harvard Global CMT Catalog at http://www.globalcmt.org/CMTsearch.html). The second, occurred on 9 September, 1998 was located in the Monte Pollino area with a magnitude M_w=5.6 (Fig. 1). Focal mechanism solutions are consistent with an oblique strike-slip mechanism and with an oblique-slip normal faulting for the above events, respectively. These mechanisms fit well with average fault plane solutions of crustal earthquakes in Southern Italy (Frepoli and Amato, 2000). We also recorded radon anomalies for the M_D=2.6 local earthquake of 20 November, 1998, which was the most energetic of that year below the Somma caldera (cf. Vilardo et al., 1999). Figure 2 shows the positive relation between Rn emissions and altitude. In particular, stations 9 and 2 are the most active ones, being located along the NNE-SSW summit fault, at about 100 to 200 m from the active fumaroles that outcrop within the eastern side of the crater. This feature further supports the idea that radon, during its upward migration, is associated with water and CO_2 (e.g., Gauthier et al., 1999).

FIG. 2

In Fig. 3 we show the cumulative activity of radon measured on the three subsets plotted against time. According to Fig. 3a and Fig. 3b an increase in radon activity (up to about 5 and 7 Bq/l) occurred just before, during and after two regional earthquakes (18 May and 9 September) magnitude $M_w > 5$. These variations were registered by the sampling sites located along the two major faults, whose roots extend down to 5-6 km into the Mesozoic basement rocks (Cassano and La Torre, 1987; Bianco et al., 1998). The stations along the caldera showed only moderate fluctuations with partial cumulative emissions ranging from 0.4 to 2.5 Bq/l (Fig. 3c). The Monte Pollino seismic event follows the local earthquake of September 8,1998, with the focus below Mount Vesuvius at 1.9 km b.s.l., and magnitude M_D=2.3 (Vilardo et al., 1999a). Our network registered the combined effect of these two and, possibly, other local seismic events, since, according to the cited authors, there has been a moderate increase in the number of minor volcanic tremors during September 1998. Finally, the striking correlation of the radon anomalies recorded during November 1998 for the three main structural units (faults and caldera), can be related to the shallow (2-2.4 km b.s.l.) and local seismicity typical of that month. The onset of the local earthquake of 11 November, 1998, with M_D=2.5, considerably increased the release of seismic energy which, in turn, culminated with the seismic event of November 20 (M_D=2.6): the most energetic of that year (cf., Vilardo et al., 1999).

This crisis was also accompanied by an increase in CO_2 concentration within the active fumaroles which reached a seasonal maximum (Chiodini et al., 1999).

FIG. 3

In the light of the above data, Cigolini et al. (2001) discriminated regional earthquakes from local seismic events: the firsts induce marked radon anomalies at the summit faults and small anomalies at the caldera bottom, whereas the seconds cause radon anomalies of *similar magnitude* at all the above structural units (the summit faults plus the caldera bottom).

In Fig. 4 we report cumulative radon activities registered before, during and after the regional event of May 19, 1998, along the NNE-SSW fault and the caldera bottom. These data suggest a moderate increase (along the fault) to minor increase (within the caldera) in radon activity few days before the onset of a regional seismic event that perfectly coincides with peaks in radon emissions. The amount of time elapsed before radon anomalies reach their maximum values is approximately 3 days, which is shorter then ^{222}Rn half life (being $t_{1/2}$ = 3.82 days). Peak values are followed by a slower decrease in radon emissions until ^{222}Rn concentrations reach background values. The time elapsed for this decline is about 3.5 longer than the above, thus bringing the total duration of the anomalies (since their early evidence) to about 13.5 days. The decrease follows an exponential law typical of the release of *pore-pressure perturbations*.

FIG. 4

Hydrodynamic parameters at Somma-Vesuvius

It is generally accepted that the upward migration of radon is ruled by convection within a porous medium (e.g., Mogro-Campero and Fleischer, 1977). The basic condition to allow fluid convection requires the Raleigh number $R_a > 4\pi^2$. In turn, R_a is related to permeability by the equation (Lapwood, 1948)

$$kgH^2\left(\frac{dT}{dz}\right)\left(\frac{d\rho_f}{dT}\right) = R_a D_m \eta \qquad (1)$$

where k is the hydraulic permeability of the porous medium, g is the acceleration of gravity, H is the height of the convective cell, dT/dz is the local temperature gradient, $d\rho_f/dT$ is the change in fluid density with temperature, D_m is the thermal diffusivity of the fluid filled medium, and η is the mean viscosity of the fluid. Recalling that $D_m = K/\rho_m C_m$ (where K is the thermal conductivity of the porous medium, ρ_m is its density and C_m is its specific heat), by introducing the coefficient of thermal expansion of the fluid α, and setting $G_T = dT/dz$, equation (1) may be solved for the Raleigh number according to

$$R_a = C_m \rho_m k \rho_f \alpha g H^2 G_T / \eta K \qquad (2)$$

At Somma-Vesuvius the height of the convective cells is 3-3.8 km because the volcanic tremor clusters at about 2-2.5 km b.s.l. (Ventura and Vilardo, 1999a) and the height of the volcanic cone is 1281 m a.s.l.. We can also assume that the fluid has a nearly constant temperature as a result of an adiabatic rise throughout most of its ascent, until it expands and cools just before reaching the surface (cf., Chiodini and Marini, 1998), so that temperature-dependant variations in density and viscosity will be minimized. The local temperature gradient is ~100 °C/km, this value being consistent with the results of high-resolution seismic tomography (Zollo et al., 1998) and mineral stabilities found within the ejected materials of the thermometamorphic contact aureole (Barberi and Leoni, 1980; Belkin et al. 1985; Fulignati et al., 1998). Thus, thermophysical parameters for the aqueous fluids have been taken to be consistent with a temperature of 300 °C (Chiodini et al., 2001). By using the values reported in Table 1, the calculated Raleigh number is R_a = 136080, well above $4\pi^2$. The maximum vertical flow rate within a confined porous medium can be approximated by (Cathles, 1998),

$$J_z \approx \sqrt{2} K (R_a - 4\pi^2)^{1/2} / \rho_f C_f H \qquad (3)$$

where C_f is the fluid specific heat. Since fluid motion is controlled by porosity, ϕ, and the true velocity of the pore fluid is $v_f = J_z / \phi$, we must select a value of porosity necessary to bring radon up to the surface before its partial decay (i.e., within $t_{1/2}$ = 3.82 days). Therefore, by setting C_f=5.4x10^3 J/kg °C (Cathles, 1998; Lemmon et al., 2005), and solving the above relationship for J_z / ϕ, we estimated a value of porosity of the order of ϕ=1.7x10^{-5}. The true velocity of the pore fluid is J_z / ϕ ≈833 m/day. However, it can be easily noted that the flow rate J_z is independent from the height of the cells since H is included both in the nominator and the denominator of the above equation. To have a more realistic estimate of porosity and permeability we may consider a NaCl aqueous fluid (Chiodini et al., 2001). According to Tanger and Pitzer, 1989, the expected NaCl contents in the vapour phase range between maximum values of 8400 to 23,800 mg/kg, for a salinity of the hydrothermal liquid phase of 3 m at pressures of 35-40 MPa. Thus, I considered a fluid mixture of 5 % NaCl, exaggerated to take into account a salt fraction inherited from the interaction of the ascending fluid with the hydrothermal brines that fill the fractures network. Assuming ideal mixing between the two

components, by utilising the data on halite (Robie et al., 1979) together with those of Lemmon et al. (2005) for pure water (cf., Table 1), I refined the estimates of wall rock porosity and permeability by calculating the thermophysical parameters of the fluid mixture reported in Table 1. Fluid viscosities were estimated at *T,P,X* by introducing the algorithm of Palliser & McKibbin (1998) for fluid mixtures at temperatures less than 800 °C:

$$\eta_{f\ mix}(T,P,X) = \frac{\eta_w(T,P)(1+3X)\left[(800-T)/800\right]^9 + (T/800)^9\left[\eta_w(T,P)(1-X)+\eta_{NaCl}(800)X\right]}{\left[\frac{800-T}{800}\right]^9 + \left(\frac{T}{800}\right)^9} \qquad (4)$$

where η_w is the viscosity of pure water at the temperature and pressure of interest (*T,P*), and *X* is the mass fraction of NaCl in the fluid mixture; η_{NaCl} is the viscosity of pure NaCl at 800 °C, i.e., $\eta_{NaCl}(800) = 4.71624\times10^{-3} - 4.0203\times10^{-6}\cdot800$.

FIG. 5, TABLE 1

Thus, the upper estimate for the viscosity of the aqueous fluid mixture leads to $\eta_{f\ mix}$ = 1.34 x 10^{-4} Pa s (Table 1). Taking into account that the total duration of ^{222}Rn anomalies (13.5 days, Fig. 6), porosity is 1.2 x $10^{-5} \leq \phi <$ 4.4 x 10^{-5}, for radon to reach the surface within 3.6 and 13.5 days, respectively. In this case fluid velocities are constrained 780 m/day$\geq v_f >$220 m/day. This relatively low porosity indicates that flow motion is strongly localised along fractures. This is consistent with the geology and the tectonic setting (Ventura and Vilardo, 1999a, b). The *k*-value used in equation (1) and (2) is a realistic estimate of the bulk permeability *for rocks lying above* a depth of 2-2.5 km b.s.l. (Table 1) being in good agreement with those measured in igneous rocks and limestones (Freeze and Cherry, 1979). In addition, rock permeabilities at depth of 2-2.5 km b.s.l. may be obtained from the well known expression $k=\alpha^*\eta\phi\beta$, where α^* the hydraulic diffusivity of the porous medium and β is the fluid compressibility. Hydraulic diffusivities have been calculated by Ventura and Vilardo (1999a) from multiple analyses of time-harmonic pore-pressure perturbations associated to volcanic tremors and earthquakes (with hypocentral depths clustering at 2-3.5 km b.s.l.). Their solutions ($0.1\leq\alpha^*\leq0.56$ m^2 s, with α^*=0.25 m^2 s being their best estimate) refer to a stress-affected porous medium under "transient conditions" induced by fluctuations of the pore-pressure front. By substituting the previous estimate of porosity (ϕ=1x10^{-5}) together with the following values: η=10^{-4} Pa s, β=2x10^{-8} Pa^{-1}, and $0.1\leq\alpha^*\leq0.25$ m^2 , the estimated value of permeability is 2x$10^{-18} \leq k \leq$ 5x10^{-18} m^2.

These low values of rock-permeability may reflect the periodic self-sealing of the deeper hydrothermal system. As pointed out by Hanson (1995) the maximum permeability to keep the fluid pressure near the lithostatic pressure ($P_f \approx P_l$) is typically about 10^{-18} m^2. The use of lower values of viscosity (typical of higher temperature fluids) would give lower estimates of permeability, that are consistent with the onset of fluid pressure build-up below a *low-permeability horizon* . Therefore, the estimates for this parameter may be regarded as "threshold values", indicating that the system, may be easily perturbed (Matthäi and Roberts, 1997). By using the higher values of hydraulic diffusivity obtained by Ventura and Vilardo (1999a), α^*=0.56 m^2, we may have an estimate of permeability under "transient conditions", i.e. k=1.1 x 10^{-17} m^2. These values would therefore describe the onset of expansion of fractures within the low-permeability horizon, inducing leaking of high pressure fluids through the rocks. It is not excluded that this conditions could be persistent in some sectors of the hydrothermal system and act like "safety valves", thus controlling progressive degassing of deep higher-temperature fluids.

A double-convective cell model for the hydrothermal system

I explored the possibility of considering a *double-convecting cell model* for the deep hydrothermal system at Somma-Vesuvius (Fig. 6).

FIG. 6, TABLE 2

As previously reported, Chiodini et al. (2001) estimated that some high-temperature fumarolic fluids (up to about 450 °C), are in equilibrium with NaCl hydrothermal brines at depth. Thus, I calculated the equilibration pressures for the data of Chiodini et al. (2001) by using the Modified Redlich Kwong (MRK) equations to estimate the maximum depth for the separation of these fluids from their hydrothermal brines. In performing these calulations I used the regular solution model for H_2O-CO_2 mixtures (Holloway, 1977; Kerrick and Jacob, 1981). The majority of the calculated fugacity coefficients for CO_2 (f_{CO_2}) are only 10-25 % off from those estimated by Chiodini et al. (2001). The results are reported in Table 2, and show that high temperature fluids coexisting with NaCl hydrothermal brines equilibrate at pressures between 1560 and 1610 MPa. Assuming an average density of 2700 Kg/m^3 for the rocks underlying Somma-Vesuvius, as suggested by the gravimetric data of Cassano and La Torre (1987) for the upper units, and those of Tondi and De Franco (2003) for lower units (3000 kg/m^3 below 3 km depth) these pressures regimes are consistent with maximum average depths of 5.7-5.9 Km for the above equilibria. This depth represents the maximum hypocentral depth of the Vesuvius earthquakes

(e.g. Lomax et al., 2001) and constrain the mean geothermal gradient at 80 °C ≤ G_T ≤ 100 °C.

In order to have an estimate of the hydrodynamic parameters that rule the upward motion of these fluids, we need to discuss a model that includes an upper convecting cell (down to 2 km b.s.l., i.e., ΔH_{uc}=3 km) and a lower convecting cell (of ΔH_{lc}= 2.8 km, due to the fact that below 3 km depth the average rock density would increase of ~10%, from 2700 to about 3000 kg/m^3; cf., Tondi and De Franco, 2003; Borgia et al., 2005). The two cells are separated by a low permeability horizon (with $k \cong 10^{-18}$ m^2, or lower) that allows moderate degassing of the high-temperature fluids through fractures acting like *safety valves* where permeability locally increases to $k \approx 10^{-17}$ m^2. A sketch illustrating this model is reported in Fig.6.

According to this model the bulk porosity may be defined as:

$$\phi_{bulk} = \phi_{uc} (\Delta H_{uc} / H_{total}) + \phi_{lc} (\Delta H_{lc} / H_{total}) \qquad (5)$$

where H_{total} is the sum of the height of the upper an lower cells ($\Delta H_{uc} + \Delta H_{lc}$= 5.8 km). Thus, the single contribution to the bulk porosity is proportional to the height of a single cell. Assuming that the fluid is allowed to flush through the "low permeability" horizon located at 2 km depth b.s.l. (recalling that the height of the volcanic cone is 1281 m a.s.l.), the time taken by the fluid to reach the surface will be

$$\Delta t_{total} = [\Delta H_{uc} / (J_{z(uc)} / \phi_{uc})] + [\Delta H_{lc} / (J_{z(lc)} / \phi_{lc})] \qquad (6)$$

Densities, viscosities and specific heats for water are reported in Fig. 5 according to the database of Lemmon et al. (2005; see http://webbook.nist.gov), which also include thermophysical data in the supercritical region. In this case I consider a fluid rising adiabatically with a temperature of 450 °C.

By forcing the fluid to reach the surface before a considerable amount of radon decay: that is by setting t_{total} =3.82 days and t_{total} =13.5 days (the half-life of ^{222}Rn and the total length of radon anomalies, respectively) together with the input parameters listed in Tables 3 and 4, the estimate for bulk porosity throughout the whole hydrothermal system is 5.3 x $10^{-6} \leq \phi_{bulk} \leq$ 6.15 x 10^{-6} for both pure water and the halite bearing-water mixture with a salinity of 2 % NaCl. The latter value is consistent with the previously discussed data of Tanger and Pitzer (1989) for a vapor phase in equilibrium with a hydrothermal liquid phase. Moreover, higher salinities will lead to higher fluid viscosities so that convection is inhibited (since the condition $R_a \geq 4\pi^2$ will not be satisfied for the lower cell). Porosities within the lower cell are estimated to be from one to two orders of magnitude lower than those calculated for the upper cell (Tab. 3 and 4) indicating that fluid motion is controlled by the fracture network associated with active faulting. In particular, I get 2.75 x $10^{-7} \leq \phi_{lc} \leq$ 1.6 x 10^{-6} for pure water, and 2.8 x $10^{-7} \leq \phi_{lc} \leq$ 2 x 10^{-6} for the NaCl-H_2O

fluid mixture that reach the surface within 3.82 and 13.5 days (the upper cell porosity being fixed at $\phi_{uc} = 1 \times 10^{-5}$). These very low porosity values within the lower cells are consistent with the "plastic behaviour" of the wall rocks associated with viscous creeping, due to the high temperatures and compaction of the brine-rich porous medium (cf., Fournier, 1999). In order to keep a convective regime within the lower cell, permeabilities need to be of the order of $k_{lc} \cong 10^{-15}$ m^2 since lower permeabilities would cause the Rayleigh number to drop below $4\pi^2$. These estimates need to be considered as a first approximation and could be better constrained in the light of additional geophysical and geochemical data. Nevertheless, the above permeability is well above $k \approx 10^{-18}$ m^2 and it is sufficient to promote convection (Table 3 and 4). However, permeability may periodically reach minimum values along the interface zone that separates the two convecting cells. This zone, likely located along the contact between the lower volcanic units and the Tertiary carbonate basement is not only a stratigraphic discontinuity, but is also a layer where the two convecting cells converge. Here, both fluids (convecting at upper and lower levels), percolating through the wallrock, will release their brines. It is therefore likely that some lower temperature fluids (350-370 °C, sampled by Chiodini et al., 2001), which equilibrate with NaCl rich brines at lower pressures, inherited their higher salinity from interaction with sea water (cf. δD vs. δ^{18}O plot by Chiodini et al., 2001; Fig. 10). In particular, Celico et al. (2001) have shown that the high salinity of groundwaters in the Neapolitan area can be explained by interaction of spring waters with sea waters carried by deep fluids. According to these authors this phenomenon occurs in proximity of tectonically complex volcanic areas that exhibit a rather high geothermal gradient, such as Vesuvius and Campi Flegrei.

TABLE 3 & TABLE 4

Cyclic seismicity and its bearing with the eruption mechanism

Several phenomena generally precede the onset of major eruptions. These include degassing, increase in seismic activity, slope deformations, fault reactivation, and gravity changes (e.g., Tilling, 1995). Similarly, precursory phenomena associated with phreatic eruptions involve anomalous seismicity (including seismic tremors as short-term precursors), ground deformation, compositional and temperature changes in fumaroles and thermal springs (Barberi et al., 1992).

Phreatic eruptions are connected with perturbations of the hydrothermal system and may be followed by magmatic and phreatomagmatic eruptions. Currently, only 19 historical phreatic events, including those occurred at Unzen, Pinatubo and Mount Saint Helen, were followed by a major eruption with the involvement of magma (Barberi et al., 1992). These authors also stressed that the small number of such cases is likely due the fact that "reporters were distracted from the comparatively minor phreatic phenomena that preceded" major eruptions. Recently,

Barberi and Carapezza (2002) pointed out that many recent magmatic or phreatomagmatic events in island arcs were preceded by phreatic explosions.

The mechanism of phreatic eruptions has been oulined by Germanovich and Lowell (1995). They show that the condition for generating these events are the following: the country rock strength should approach 10 MPa. It should be characterised by a *two-permeability structure* involving a main crack network of "higher" permeability (similar to 10^{-12} m^2), and a *subsidiary network* bearing disconnected cracks with much lower permeability ($<10^{-17}$ m^2). Del Pezzo et al. (2004) have shown that the stress released during the onset of major local earthquakes reaches values of ~ 10 MPa at 2-3 km depth below Vesuvius (i.e., at the top of the carbonate basement). In addition, the permeability values provided by Germanovich and Lowell (1995) are consistent, within one order of magnitude, with those estimated for the upper convective cell (10^{-12} m^2) and the lower permeability horizon (with $k \approx 10^{-18}$ m^2, or lower) at Vesuvius. Therefore, the overall structural setting of the volcanic edifice well fits with the constraints of Germanovich and Lowell (1995). In the Vesuvius case, the *loci* of hydrodynamic disequilibria, that may lead to phreatic explosions, are located between the upper convecting cell and the low permeability horizon. This zone is the one affected by higher stress regimes because fluid pressure build up will occur essentially below the low-permeability horizon. According to Germanovich and Lowell (1995), the ascending superheated steam will induce boiling of the fluid residing in the subsidiary crack network. The increase in pressure, exerted by the vapour, may lead to rapid crack propagation that, in turn, lowers the rock tensile strength and may trigger a phreatic eruption promoted by domains of thermoelastic isostresses. However, depending on local rock parameters, crack propagation may simply generate highly cracked zones that could later be "sealed" by uprising fluids. This seems to be the process presently active at Somma-Vesuvius that basically explains cyclic seismicity. FIG. 7

Thus, the current cyclic seismicity at Somma-Vesuvius is ruled by a *feedback mechanism* that modulates the dynamics of the hydrothermal system (cf. Cigolini et al., 2001). This mechanism is summarised in Fig. 8 and can be described as follows: fluid pressure build up (below a low permeability horizon, with $k \approx 10^{-18}$ m^2)$\rightarrow$ fluid release and migration during incipient fracturing of the porous medium (Hishimuma et al., 1999)[1]$\rightarrow$ failure of the porous medium triggering local earthquakes$\rightarrow$ fluid circulation and progressive self-sealing of the "deep"

[1] They experimentally analyzed the emission of thoron in small-scale crushing experiments. The short-lived thoron has been considered a better indicator for investigating the onset of anomalies. The results show a slight increase in thoron emissions during sample compression, followed by a drastic increase during and after failure of the sample. After complete crushing the emission of thoron progressively reduces to zero.

hydrothermal shell, until critical permeabilities are reached to prevent further degassing. In tectonically active areas such a mechanism is also known as crack-seal (Petit et al., 1999).

The whole cycle may be periodically reactivated, and besides static and dynamic triggering induced by regional tectonic earthquakes (e.g., Nostro et al., 1998; Hill et al., 2002), astronomical factors may be involved in the activation process as well (e.g., Sparks 1981; Duma and Vilardo, 1998).

Anomalous pressure build-ups could induce hydraulic surge with extensive hydrofracturing (e.g., Fourniere, 1999; Hill et al., 2002) eventually leading to phreatic eruptions. If local seismic crises will reach threshold values, characterised by magnitudes somehow higher than the major ones occurring below Somma-Vesuvius ($M_L \geq 3.6$, with a minimum stress release of ~ 10 MPa), it is not excluded that these processes could reactivate the summit "quiescent" faults inducing pervasive failure of the hydrothermal shell (Ventura and Vilardo, 1999b). This mechanism may eventually depressurize the magma chamber favouring dike emplacement thus triggering magmatic eruptions (e.g., Jellinek and De Paolo, 2004).

Discussion and conclusions

Vesuvius cyclic seismicity could be explained by means of a double-convective cell model. The two convective cells are separated by a low permeability horizon located at about 2 km below sea level. This horizon is a layer where the two convecting cells converge and the fluids (convecting at upper and lower levels) normally release their brines. Permeabilities within this layer are minimised due to self-sealing processes and reach the critical values of $k \approx 10^{-18}$ m^2 to keep the fluid pressure near the lithostatic pressure ($P_f \approx P_l$). Fluid pressure build ups, followed by fluid release and migration during incipient fracturing of the porous medium, precede the onset of hydrothermally-induced earthquakes. Anomalous pressure build-ups may induce extensive hyrofracturing eventually leading to hydraulic surges which may evolve into phreatic eruptions. However, the hydrothermal dynamics of Somma-Vesuvius could also be perturbed by static or dynamic stresses induced by regional earthquakes.

The involvement of a hydrothermal acquifer during the *final stage* of earlier eruptions (1631-1944) has been recognised by several authors (Santacroce, 1987; Bertagnini et al., 1992; Arrighi et al., 2000). These authors identified abundant lithic fragments of hydrothermalised lavas and dykes that occur in phreatomagmatic ash layers laying on top of juvenile tephra. In addition, mineral assemblages found in lithic fragments from plinian and subplinian eruptions (A.D. 79 to 472) indicate that the hydrothermal system reached temperatures of 360-400 °C (Fulignati et al., 1995), which are in good agreement with the temperatures inferred by Chiodini

and Marini (1998) and Chiodini et al. (2001) for the deep fluids associated with the current hydrothermalism. Nevertheless, pressure build ups below the low permeability horizon may lead to the onset of hydrualic surges. During their early stage, eruptions could be essentially phreatic but they could evolve into magmatic and phreatomagnatic eruptions, depending on the developing of seismic sequences and/or the energy of local earthquakes.

In conclusion, radon monitoring is a very powerful tool to decode the dynamic behaviour of deep hydrothermal systems and to analyse the precursory hydraulic and/or phreatic phenomena that may lead to magmatic and/or phreatomagmatic eruptions in active volcanic areas. A fully automated network, with stations operating continuously and contemporaneously, will contribute to further refine the correlation between radon emmissions and local seismicity, definitely improving volcano surveillance.

The methodology hereby presented, which involves an integrated analysis of seismic and geochemical data, could be used to constrain variations in porosity and permeability as well as temperature distributions within active geothermal systems.

Aknowledgements

This paper was funded by the National Institute for Geophysics an Volcanology (INGV) and MIUR. A. Frepoli provided the focal mechanism solutions for the two regional earthquakes considered. A. Borgia, C. Kilburn, and G. Ventura provided helpful comments. I wish to thank the staff of the “Osservatorio Vesuviano” for the hospitality during field work

---

References

Arrighi S, Principe C, Rosi M (2001) Violent strombolian and subplinian eruptions at Vesuvius during the post-1631 activity. Bull Vocanol 63: 126-150

Auger A, Gasparini P, Virieux, J, Zollo A (2001) Seismic evidence of an extended magmatic sill under Mt.Vesuvius. Science 294: 1510-1512

Barberi F., Leoni L, (1980) Metamorphic carbonate ejecta from Vesuvius Plinian eruptions: evidence for the occurrence of shallow magma chambers, Bull Volcanol 43-1: 107-120.

Barberi F, Bertagni A, Landi P., Principe P. (1992) A review on phreatic eruptions and their precursors. J Volcanol Geothermal Res 52: 231-246

Barberi F, Carapezza ML (2002) Phreatic eruptions at converging plate volcanoes: isolated minor events or forerunners of major eruptive bursts. In “Explosive volcanism in Subduction Zones, Mount Pelée 1902-2002”, 76

Belkin HE, De Vivo B, Roedder E, Cortini M (1985) Fluid inclusion geobarometry from ejected Mt. Somma-Vesuvius nodules. Am Mineral 70: 228-303.

Bertagnini A, Landi P, Santacroce R, Sbrana A (1991) The 1906 eruption of Vesuvius from magmatic to phreatomagmatic activity through the flashing of a shallow depth hydrothermal system. Bull Volcanol 53 (7): 517-532

Bianco F., Castellano M, Milano G, Ventura G, Vilardo G (1998) The Somma-Vesuvius stress-field induced by regional tectonics.: evidences by seismological and mesostructural data. J Volcanol Geothermal Res 82: 199-218

Bonetti R., Capra L, Chiesa C, Guglielmetti A, Migliorini C (1991) Energy response of LR115 cellulose nitrate to alpha particle beams, Nuclear Radiation Measurements. 18: 321-338

Borgia A, Tizzoni P, Solaro G, Manzo M, Casu F, Luongo G, Pepe A, BerardinoP, Fornaio G, Sansosti E, Ricciardi GP, Fusi N, Di Donna G, Lanari R (2005) Volcanic spreading of Vesuvius, a new paradigm for interpreting its volcanic activity. Geoph Res Lett 32: Art n L03303

Burton M, Neri M, Condarelli D (2004) High spatial resolution radon measurements reveal hidden active faults on Mt. Etna, Geoph Res Lett 31 Art n L07618

Cassano E., La Torre P (1987) Geophysics, In Somma-Vesuvius. Santacroce R. (ed). CNR Quad Ric Sci 114/8, pp. 175-196

Cathles LM (1997) Thermal Aspects of Ore Formation, In Geochemistry of Hydrothermal Ore Deposits. Barnes HL (ed). John Wiley & Sons, New York, pp. 191-227.

Celico F., Esposito L, Mancuso M (2001) Hydrodynamic and hydrochemical complexity of Naples urban area: some interpretations. Geologia Tecnica & Ambientale 2: 35-54.

Chiodini G, Marini L (1998) Hydrothermal gas equilibria: The H2O-H-2-CO2-CO-CH4 system.
Geochim Cosmochim Acta 62 (15): 2673-2687

Chiodini G, Avino R, Cardellini C., Caliro S, Granieri G, Russo M (1999) Geochimica. Rend Att Sorveglianza Oss. Vesuviano: pp. 26-29

Chiodini G., Marini L., Russo M., 2001. Geochemical evidence for the existence of high-temperature hydrothermal brines at Vesuvio volcano, Italy. Geochim. Cosmochim. Acta 65 (13): 2129-2147.

Chirkov AM (1975) Radon as a possible criterion for predicting eruptions as observed at Karymsky volcano. Bull Volcanol 39 (1): 126-131.

Cigolini, C, Salierno F, Gervino G, Bergese P, Marino C, Russo M, Prati, P, Ariola V, Bonetti, R, Begnini S (2001) High-resolution Radon Monitoring and Hydrodynamics at Mount Vesuvius. Geoph Res Letters 28: 4035-4039

Cigolini C, Gervino G, Bonetti R, Conte F, Laiolo M, Coppola D, Manzoni A (2001) Tracking precursors and degassing by radon monitoring during major eruptions at Stromboli Volcano (Aeolian Islands, Italy). Geoph Res Lett 32 art n L12308

Connor C, Hill B, LaFemina P, Navarro M, Conway M (1996) Soil Rn-222 pulse during the initial phase of the June August 1995 eruption of Cerro Negro, Nicaragua. J Volcanol Geothermal Res 73 (1-2): 119-127

Cox ME (1980) Ground Radon Survey of a Geothermal area in Hawaii, Geoph Res Letters, 7: 283-286

Cox, M.E, 1983. Summit outgassing as indicated by Radon, Mercury and pH mapping, Kilauea Volcano, Hawaii, J. Volcanol. Geothermal Res., 16: 131-151

Del Pezzo E, Blanco F, Saccorotti G (2004) Seismic source dynamics at Vesuvius volcano, Italy. J Volcanol Geothermal Res 133 (1-4): 23-39

Del Moro A, Fulignati P, Marianelli P, Sbrana A (2002) Magma contamination by direct wall rock interaction: constraints from xenoliths from the walls of a carbonate-hosted magma chamber (Vesuvius 1944 eruption). J Volcanol Geothermal Res 112 (1-4): 15-24

De Natale G, Kuznetzov I, Kronrod T, Peresan A, Sarao A, Troise C, Panza GF (2004) Three decades of seismic activity at Mt. Vesuvius: 1972-2000. Pure and Applied Geoph 161 (1): 123-144

De Natale G, Troise C, Pingue F, Mastrolorenzo G, Pappalardo L (2006) The Somma-Vesuvius volcano (Southern Italy): Structure, dynamics and hazard evaluation. Earth Sci Rev 74 (1-2): 73-111

Di Maio R, Mauriello P, Patella D, Petrillo Z, Piscitelli S, Siniscalchi A (1998) Electric and electromagnetic outline of the Mount Somma-Vesuvius structural setting. J. Volcanol Geothermal Res 82/1-4: 131-151

Duma, G, Vilardo G. (1998) Seismicity cycles in the Mount Vesuvius area and their relation to solar flux and variations of the Earth Magnetic Field. Physics and Chemistry of the Earth 23: 927-931

Federico C, Aiuppa A, Favara R, Gurrieri S, Valenza M (2004) Geochemical monitoring of groundwaters (1998-2001) at Vesuvius volcano (Italy). J. Volcanol Geothermal Res 133 (1-4): 81-104

Fleischer RL, Mogro-Campero A (1985) Association with subsurface radon changes in Alaska and the Northeastern United States with earthquakes. Geochim Cosmochim Acta 49: 1061-1071

Frepoli A, Amato A (2000) Fault plane solutions of crustal earthquakes in Southern Italy (1988-1995): seismotectonic implications. Annali Geof 43 (3) 437-467

Fournier RO (1999)Hydrothermal processes related to movement of fluid from plastic into brittle rock in the magmatic-epithermal environment. Econ Geol 94 (8): 1193-1212

Freeze RA, Cherry JA, 1979. Groundwater. Prentice Hall, Engelwood Cliffs, NJ.

Fulignati P, Gioncada A, Sbrana A (1995) The magma chamber related hydrothermal system of Vesuvius: first mineralogical and fluid inclusion data on hydrothermal subvolcanic and lavic samples from phreatomagmatic eruptions. Per Mineral 64: 185-187.

Fulignati P, Marianelli P., Sbrana A (1998) New insights on the thermometamorphic-metasomatic magma chamber shell of the 1944 eruption of Vesuvius. Acta Vulcanol. 10: 47-54

Gauthier PJ, Condomines M, Hammouda T (1999) An experimental investigation of radon diffusion in an anhydrous andesitic melt at atmospheric pressure: Implications for radon degassing from erupting magmas. Geochim Cosmochim Acta 63: 645-656.

Germanovich LN, Lowell RP (1995) The mechanism of phreatic eruptions . J Geophysical Res 100 (B5): 8417-8434

Gervino G, Bonetti R, Cigolini C, Marino C, Prati P, Pruiti L (2004) Enviromental Radon Monitoring: Comparing drawbacks and performances of charcoal canisters, α-track and E-PERM detectors in radon monitoring, Nucl Instr Meth. in Phys Res S A 518: 452-455

Hill DP, Pollitz F, Newhall C (2002) Earthquake-volcano interactions, Physics Today, 55: 41-47

Hanson RB (1995) The Hydrodynamics of contact metamorphism. Geol Soc of America Bull 107: 595-611

Hishimuma T, Nishikawa T, Shimoyama T, Myajima M, Tamagawa Y, Okabe S (1999) Emission of radon and thoron due to the fracture of rock. Il Nuovo Cimento 22/3-4: 523-527

Holloway JR (1977) Fugacity and activity of molecular species in supercritical fluids. In Thermodynamics in Geology, Fraser DG (ed), Reidel Dordrecht, Holland, pp. 161-181

Iigarashi G, Saeki S, Takahata N, Sumikawa K, Tasaka S, Sasaki Y, Takahashi M, Sano Y (1995) Ground-water Radon Anomaly before the Kobe Earthquake in Japan. Science 269: 60-61.

Jellinek AM, De Paolo D (2003) A model for the origin of large silicic magma chambers: precursors of caldera forming eruptions, Bull. Volcanol. 65: 363-381

Kerrick DM, Jacob GK (1981) A modified Redlich-Kwong equation for H_2O, CO_2 and H_2O-CO_2 mixtures at elevated pressures and temperatures. Am J Sci 281: 735-767

Lapwood ER (1948) Convection of a fluid in a porous medium. Proc Cambridge Philos Soc 44: 508-52.

Lemmon EW, McLinden MO, Friend DG (2005) Thermophysical Properties of Fluid Systems. In NIST Chemistry WebBook, NIST Standard Reference Database Number 69, Linstrom PG and Mallard WG (Eds), National Institute of Standards and Technology, Gaithersburg MD, 20899 (http://webbook.nist.gov).

Lomax A, Zollo A, Capuano P, Virieux J (2001) Precise, absolute earthquake location under Somma–Vesuvius volcano using a new 3D velocity model. Geophys. J. Int. 146: 313–331

Matthäi S, Roberts SG (1997) Transient versus continuous fluid flow in seismically active faults: an investigation by electric analogue and numerically modelling, In Fluid Flow and Transport in Rocks, Jamtveit B and Yardley BDV (Eds.). Chapman & Hall, London: 263-295

Mogro-Campero A., Fleischer RL (1997) Subterrestrial fluid convection: a hypothesis for long distance migration of radon within the earth. Earth & Planetary Science Letters 34: 321-325

Müeller M, Hördt A, Neubauer FM (1999) Electromagnetic Technique's Success at Vesuvius Points to use in Forecasting Eruptions. EOS Trans. AGU 80: 393-401

Nostro C, Stein RS, Cocco M, Belardinelli ME, Marzocchi W (1998) Two-way coupling between Vesuvius eruptions and southern Apennine earthquakes, Italy, by elastic stress transfer. J Geoph Res 103: 24487-24504

Oxburgh, E.R., 1980. Heat Flow and Magma Genesis, In Physics of Magmatic Processes, Hargraves RB (Ed) Princeton Univ. Press, Princeton, pp. 161-194

Palliser C, McKibbin R (1998) A model for deep geothermal brines III: Thermodynamic properties – enthalpy and viscosity. Transport in Porous Media, 33, 155–71

Pandolfi D, Bean CJ, Saccorotti G (2006) Coda wave interferometric detection of seismic velocity changes associated with the 1999 M=3.6 event at Mt. Vesuvius. Geoph Res Lett 33 (6): Art n L06306

Petit J, Wibberley CA.J, Ruiz G. (1999) `Crack-seal', slip: a new fault valve mechanism? Journal of Structural Geology, 21, 8/9: 1199-1207

Planicić J, Radolić V, Vuković B (2004) Radon as an earthquake precursor. Nucl Instr Meth in Phys. Res. S. A 530 568-574

Prati P., Cavagnetto F, Corvisiero P, Foppiano F, Pilo A, Salvo C, Taccini G (1992) A radon measuring technique with germanium detectors. Physica Medica VIII 1: 31-33

Robie RA, Hemingway BS, Fisher JR (1979) Thermodynamic properties of minerals and related substances at 218.15 K and 1 Bar (105 Pascals) Pressure and Higher Temperatures. U.S. Geol Surv Bull 1452, 456 pp

Sadovsky MA, Nersesov IL, Nigmatullaev SK, Latynina LA, Lukk AA, Semenov AN, Simbireva IG, Ulomov VI (1972) The processes preceding strong earthquakes in middle Asia. Tectonophysics 14: 295-307

Santacroce R. (1987) Somma-Vesuvius. Santacroce R (Ed). C.N.R. Quad Ric Sci 114/8, 251 p.

Scholtz CH, Sykes LR, Aggarval YP (1973) Earthquake prediction: a physical basis Science 181: 803-810

Sparks RSJ (1981) Triggering of volcanic eruptions by Earth tides. Nature 290: 448

Tanger JC, Pitzer K S (1989) Thermodynamics of NaCl-H2O: A new equation of state for the near-critical region and comparison with other equations for adjoining regions. Geochim. Cosmochim. Acta 53: 973–987.

Tilling RI (1995) The role of monitoring in forecasting volcanic events. In Monitoring active volcanoes McGuire E, Kilburn C and Murray J (Eds), UCL Press London, pp. 369-397

Tondi R, De Franco R (2003) Three-dimensional modeling of Mount Vesuvius with sequential integrated inversion. J Geoph Res 108 (B5): Art n 2256

Tracy RJ, Frost BR (1991) Phase equilibria and thermobarometry of calcareous, ultramafic and mafic rocks, and iron formations. Rew Mineral 26: 207-289

Ventura G, Vilardo G (1999a) Seismic-based estimate of hydraulic parameters at Vesuvius volcano Geoph Res Letters 26/7: 887-890

Ventura G, Vilardo G (1999b) Slip tendency analysis of the Vesuvius faults: implications for the seismotectonic and volcanic hazard assessment. Geoph Res Letters 26/21: 3229-3232.

Vilardo G., Bianco F, Castellano M (1999) Sismicità. Rend. Att. Sorveglianza Oss. Vesuviano, pp. 1-5

Zollo A, Gasparini P, Virieux J, Biella G, Boschi E, Capuano P, De Franco R, Dell'Aversana P, De Natale G, De Matteis R, Iannacone G, Guerra I, Le Meur H, Mirabile I (1998) An image of Mt. Vesuvius obtained by 2D seismic tomography. J Volcanol Geothermal Res 82 (1-4): 161-163

Zollo A, Marzocchi W, Capuano P, Lomax A, Iannaccone G (2002) Space and time behavior of seismic activity at Mt. Vesuvius volcano, southern Italy. Bull Seism Soc Am 92 (2): 625-640

FIGURE CAPTIONS

Fig. 1. **a)** Simplified structural setting of the Southern Italy and locations of the two tectonic earthquakes (with $M_w \geq 5$) that have been recorded during our survey. Focal mechanism solutions have been kindly provided by A. Frepoli; **b)** Structural sketch of Somma-Vesuvius and the network for radon monitoring. Sampling stations are numbered.

Fig. 2. Correlation between Radon emissions and the altitude of the volcanic cone. Higher emissions occur within the crater area. Radon activities were measured by using LR115 track-etch detectors finely calibrated for alpha particle beams. Error bars indicate 2σ uncertainties on single measurements. Track-etches were exposed from the 7th of November to the 23rd of November 1998.

Fig. 3. Correlation of radon anomalies with regional and local earthquakes. Diamonds represent average data obtained on a group of stations sampled along each single structural unit. Radon activities were measured on charcoal canisters by means of HPGe detectors (~ 7 % instrumental errors on single measurements). Dates of earthquakes are framed in the upper part of panels: the first regional event (R_1) occurred on 18 May, 1998 at 19:17 GMT, with epicenter off the Campanian coast; the second (R_2) on 9 September, 1998 at 11:28 GMT, with epicenter near Monte Pollino. The local earthquake of 20 November, 1998 (L), with M_D=2.6, may be easily discriminated since radon anomalies were recorded along the faults and the caldera bottom. Vertical lines identify the onset of earthquakes. Vertical bars represent standard deviations obtained on a given set of samples (reported only if graphically compatible with the scale used).

Fig. 4. Radon activities registered before, during and after the regional event of 19 May, 1998, along the NNE-SSW fault and the caldera bottom. The dashed lines represents average activities excluding peaks' values. The decrease in radon activity after the seismic event follows an exponential law typical of the release of pore-pressures coupled with radon decay.

Fig. 5. Variations of density (a), viscosity (b) and specific heat (c) for pure water in function of temperature and pressure. Data are from NIST Chemistry WebBook (Lemmon et al., 2005). Selected values used in calculations are reported in Table 1, 3 and 4.

Fig. 6. The inner structure of the hydrothermal system of Somma-Vesuvius with a simplified sketch of the double convective cell model. Best estimates for hydraulic parameters are also reported (see text for details). Grey thick arrows represent fluid pressure builds up below the low permeability horizon, where the critical condition $P_f \approx P_l$ could be reached before the onset of a local earthquake. Black-dashed

arrows indicate fluid motion through the low permeability horizon to equilibrate fluid pressure builds ups.

Fig. 7. Conceptual feedback mechanism for explaining cyclic seismicity at Somma-Vesuvius. Variations in rock permeabilities play a key role. Following a typical local earthquake, permeabilities would be initially higher but fluid circulation would induce progressive self-sealing of fracture networks. This would enhance fluid pressure build-up followed by incipient fracturing of the porous medium accompanied by a nearly instataneous fluid release. Failure of porous medium will again lead to the onset of Vesuvian earthquakes and so on.

FIG. 1

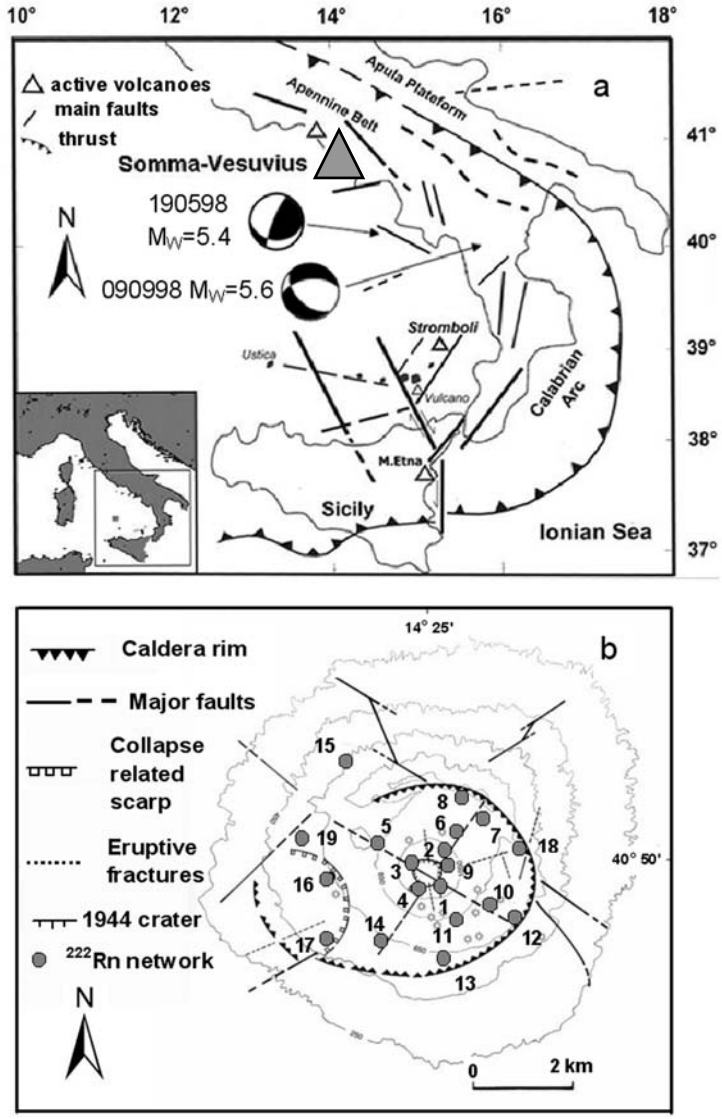

Fig. 2

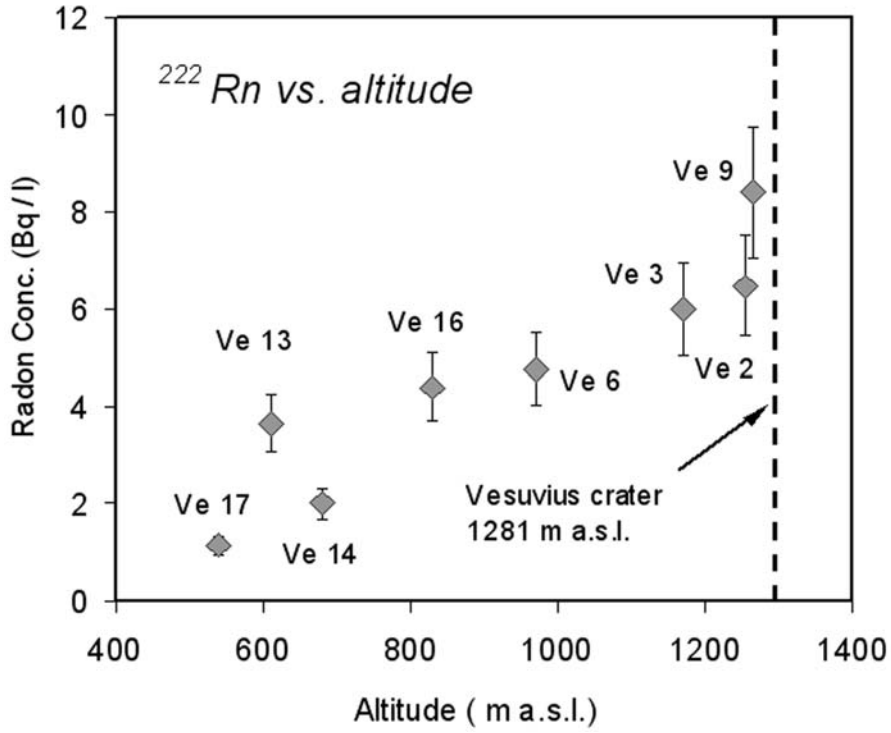
222 Rn vs. altitude
Radon Conc. (Bq / l)
Altitude (m a.s.l.)
0
2
4
6
8
10
12
400
600
800
1000
1200
1400
Ve 17
Ve 14
Ve 13
Ve 16
Ve 6
Ve 3
Ve 9
Ve 2
Vesuvius crater
1281 m a.s.l.

Fig. 3

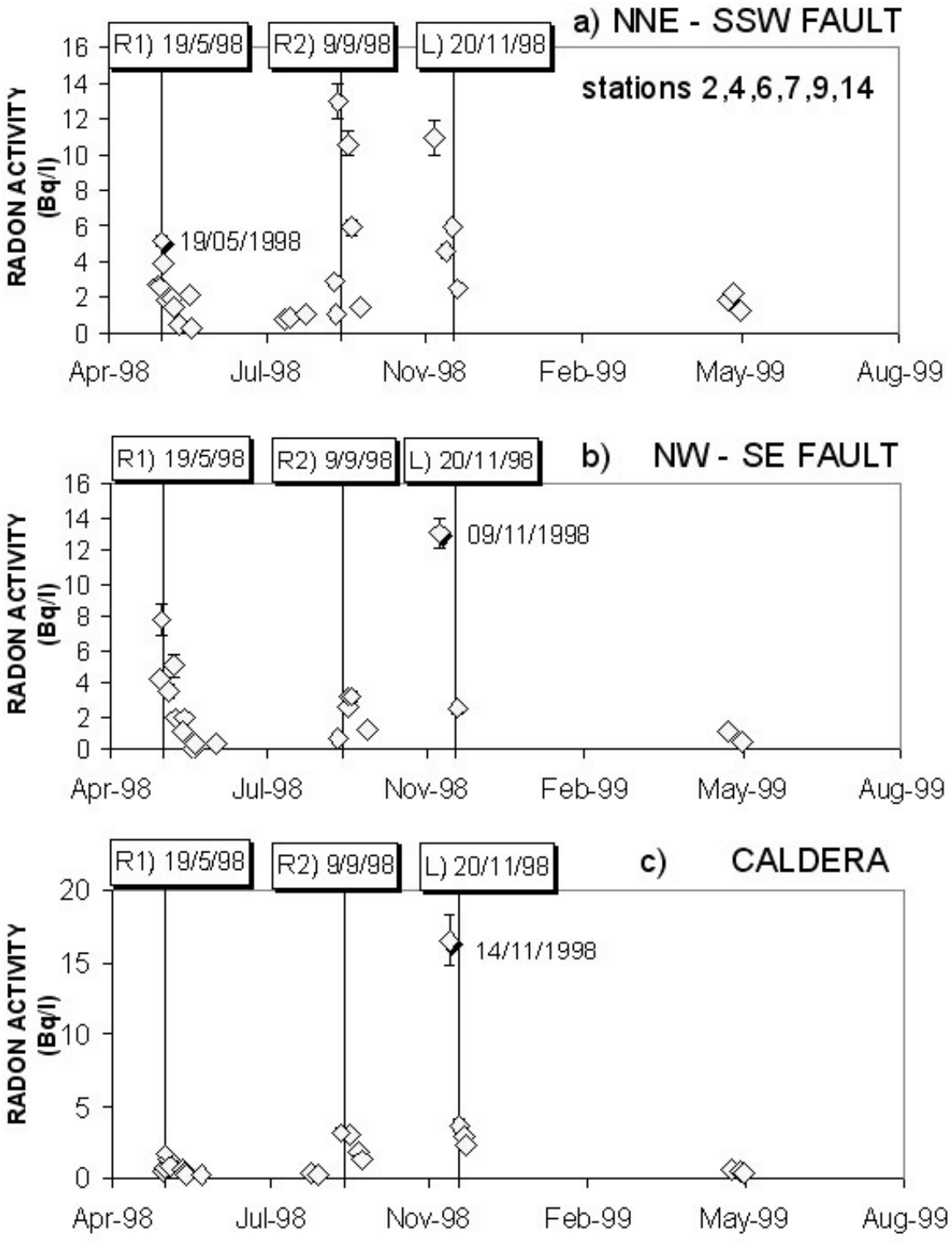
a) NNE - SSW FAULT
stations 2,4,6,7,9,14
R1) 19/5/98
R2) 9/9/98
L) 20/11/98
19/05/1998
RADON ACTIVITY (Bq/l)
0
2
4
6
8
10
12
14
16
Apr-98
Jul-98
Nov-98
Feb-99
May-99
Aug-99
b) NW - SE FAULT
R1) 19/5/98
R2) 9/9/98
L) 20/11/98
09/11/1998
RADON ACTIVITY (Bq/l)
0
2
4
6
8
10
12
14
16
Apr-98
Jul-98
Nov-98
Feb-99
May-99
Aug-99
c) CALDERA
R1) 19/5/98
R2) 9/9/98
L) 20/11/98
14/11/1998
RADON ACTIVITY (Bq/l)
0
5
10
15
20
Apr-98
Jul-98
Nov-98
Feb-99
May-99
Aug-99

Fig. 4

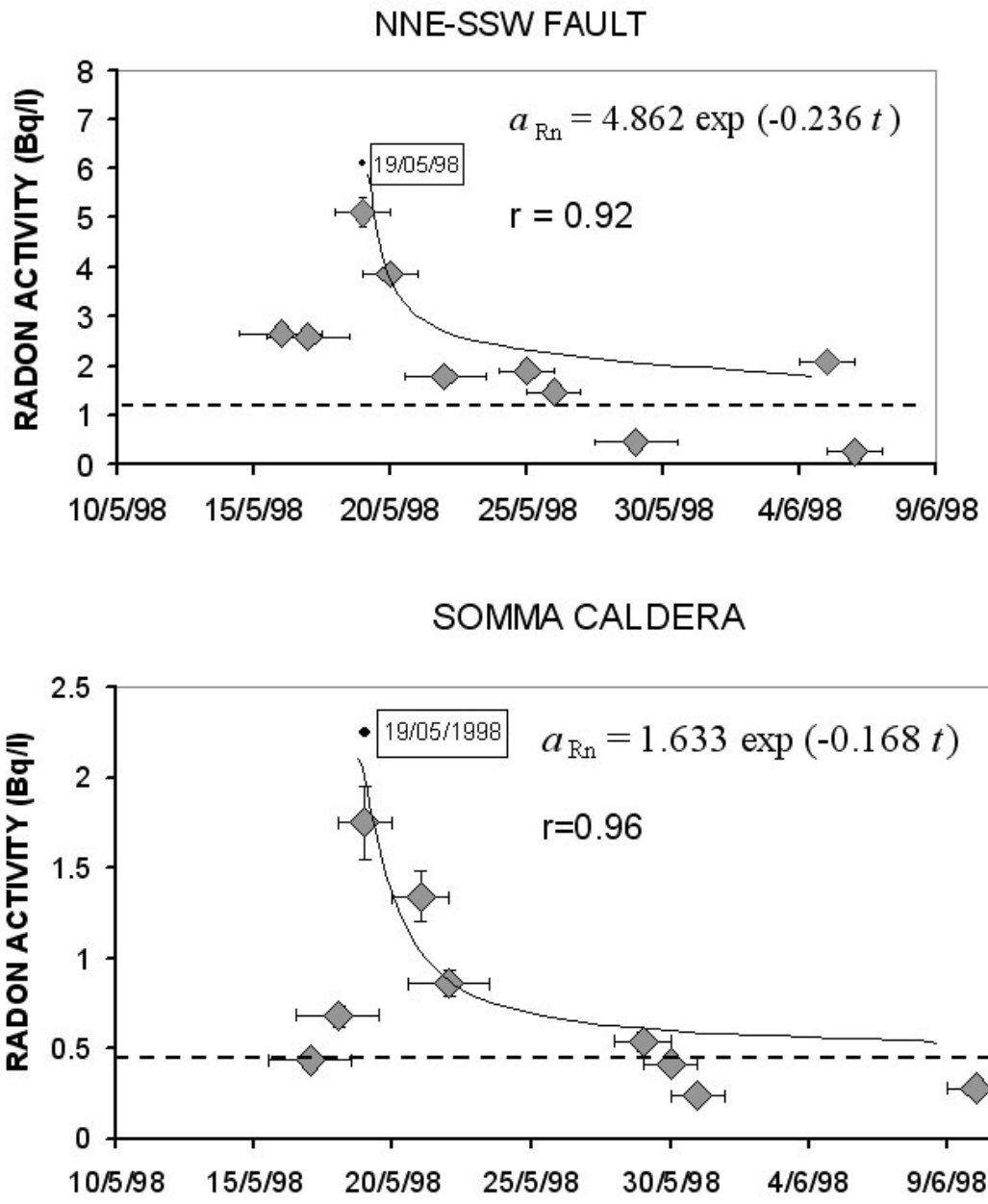
NNE-SSW FAULT
RADON ACTIVITY (Bq/l)
$a_{Rn} = 4.862 \exp(-0.236\, t)$
19/05/98
r = 0.92
10/5/98
15/5/98
20/5/98
25/5/98
30/5/98
4/6/98
9/6/98
SOMMA CALDERA
RADON ACTIVITY (Bq/l)
19/05/1998
$a_{Rn} = 1.633 \exp(-0.168\, t)$
r=0.96
10/5/98
15/5/98
20/5/98
25/5/98
30/5/98
4/6/98
9/6/98
14/6/98

Fig. 5

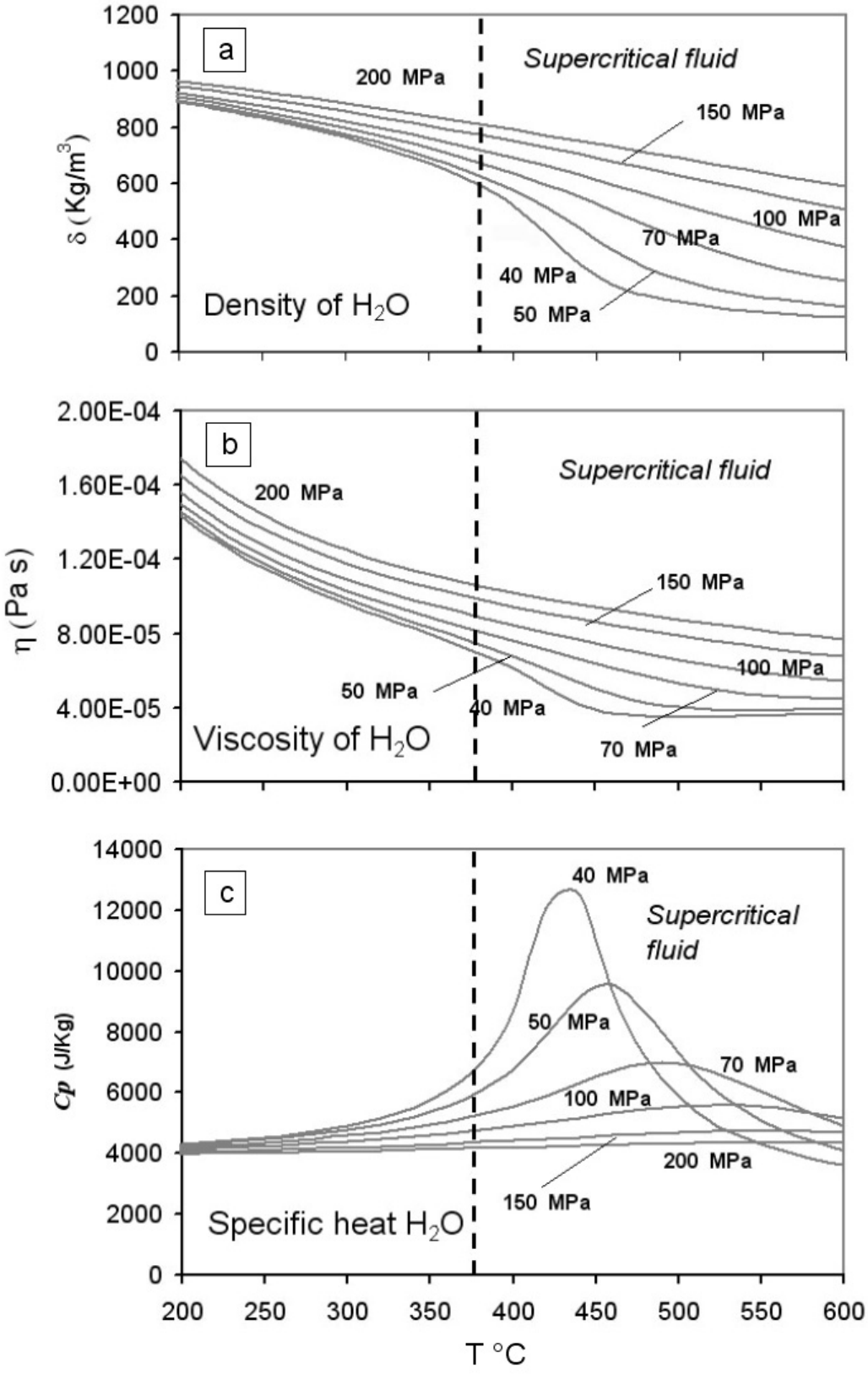
a
Supercritical fluid
200 MPa
150 MPa
100 MPa
70 MPa
40 MPa
50 MPa
Density of H2O
δ (Kg/m3)
1200
1000
800
600
400
200
0
b
Supercritical fluid
200 MPa
150 MPa
100 MPa
50 MPa
40 MPa
70 MPa
Viscosity of H2O
η (Pa s)
2.00E-04
1.60E-04
1.20E-04
8.00E-05
4.00E-05
0.00E+00
c
40 MPa
Supercritical fluid
50 MPa
70 MPa
100 MPa
200 MPa
150 MPa
Specific heat H2O
Cp (J/Kg)
14000
12000
10000
8000
6000
4000
2000
0
200
250
300
350
400
450
500
550
600
T °C

Fig. 6

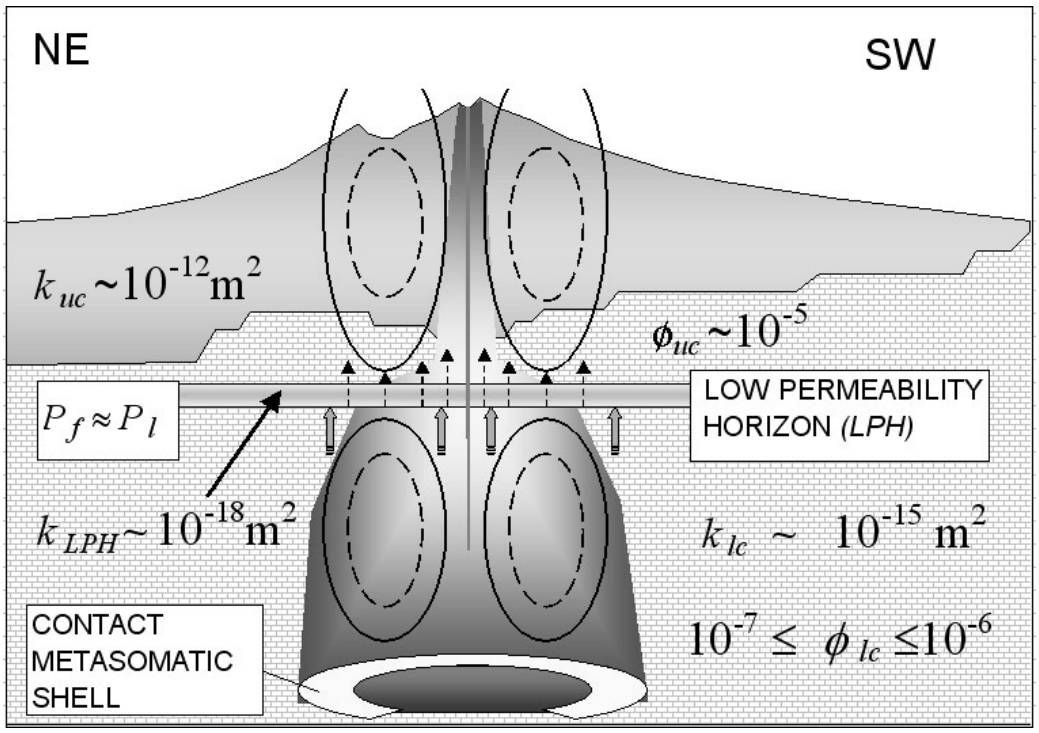
NE
SW
$k_{uc} \sim 10^{-12} m^2$
$\phi_{uc} \sim 10^{-5}$
LOW PERMEABILITY HORIZON (LPH)
$P_f \approx P_l$
$k_{LPH} \sim 10^{-18} m^2$
$k_{lc} \sim 10^{-15} m^2$
$10^{-7} \leq \phi_{lc} \leq 10^{-6}$
CONTACT METASOMATIC SHELL

Fig. 7

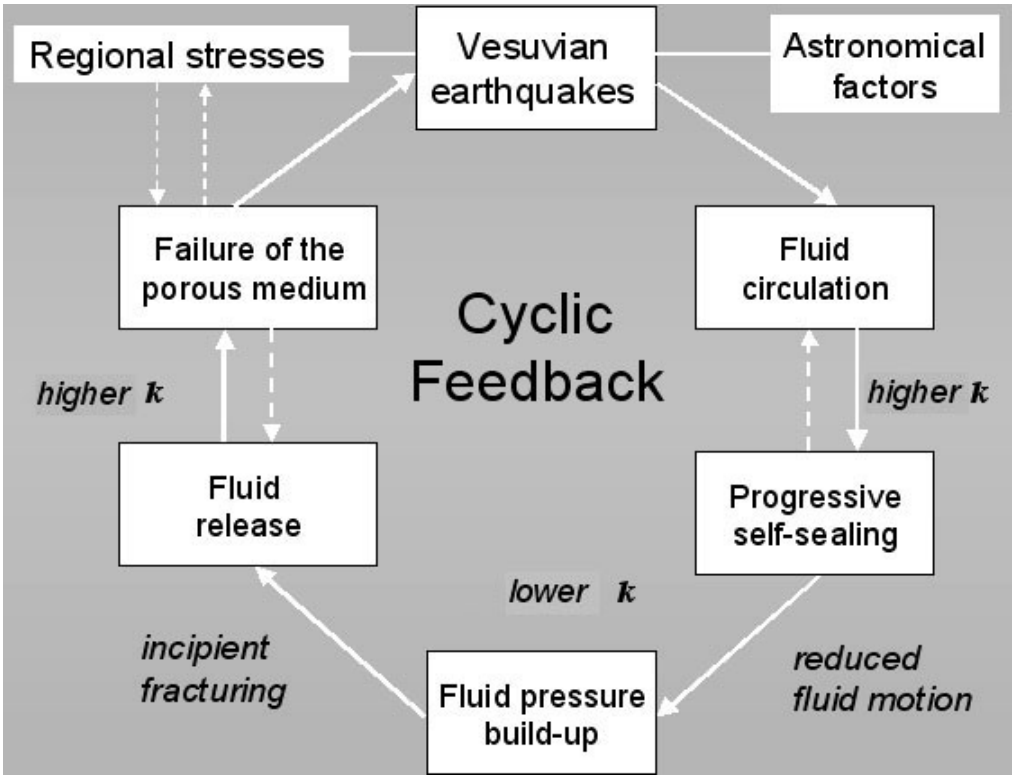
Regional stresses
Vesuvian earthquakes
Astronomical factors
Failure of the porous medium
Fluid circulation
Cyclic Feedback
higher k
higher k
Fluid release
Progressive self-sealing
lower k
incipient fracturing
reduced fluid motion
Fluid pressure build-up

Table 1. Summary of physical parameters used in estimating fluid flow rates at Somma-Vesuvius. Data for pure water are referred to 40 MPa and 300 °C (values appropriate for the centers of the convecting cells and a geothermal gradient of 100 °C/km).References support the values used in equation (1) and (2). The data for halite (NaCl) are from Robie et al. (1979). See the bottom of the table and text for details.

Symbol	Definition	Value	Ref.
POROUS MEDIUM			
ρ_m	Mean density (fluid filled medium)	2700 kg/m^3	1
k	Rock permeability	1 X 10^{-12} m^2	2
K	Rock thermal conductivity	3.5 J/m s °K	3[a]
C_m	Specific heat (fluid filled medium)	10^3 J/kg °K	4
WATER (at 40 MPa and 300 °C)			
ρ_w	Mean fluid density (water)	700 kg/m^3	5
α_w	Fluid thermal expansion (water)	2 X 10^{-3} °C^{-1}	1
η_w	Mean fluid viscosity (water)	7 X 10^{-5} Pa s	5
C_f	Specific heat (water)	5.4 X 10^3 J/kg °C	1, 5
HALITE (300 °C)			
ρ_{NaCl}	Density of halite at 300 °C	2086 kg/m^3	6
α_{NaCl}	Thermal expansion (halite)	1.3 X 10^{-4} °C^{-1}	6
C_{NaCl}	Specific heat (halite at 300 °C)	9.5 X 10^2 J/kg °K	6
MIXTURE (95 % water 5 % NaCl) at 300 °C			
$\rho_{f\,mix}$	Density of the fluid mixture	769 kg/m^3	7
$\alpha_{f\,mix}$	Thermal expansion (fluid mixture)	1.907 x 10^{-3} °C^{-1}	7
$\eta_{f\,mix}$	Viscosity (fluid mixture)	1.34 X 10^{-4} Pa s	7
$C_{f\,mix}$	Specific heat (fluid mixture)	5.18 X 10^3 J/kg °K	7

References: 1, Cassano and La Torre (1987); 2, consistent with Ventura and Vilardo (1999a); 3, Oxburgh (1980) [a]Value suggested for magnesian limestones and massive igneous rocks; 4, Cathles (1998); 5, Lemmon et al. (2005): parameters η_f, ρ_f and C_f were estimated at 40 MPa and 300 °C (see text); 6, data are from Robie et al. (1979): ρ_{NaCl} =2163 kg/m^3 at standard state, the molar heat capacity for halite is C_p = 49.151 + 1.7974 x 10^{-2} T (°K); 7, this work.

Table 2. Summary of calculations for H_2O-CO_2 mixtures assuming the regular solution models of Holloway (1977) and Kerrick and Jacob (1981). Calculations have been performed for the high temperature fluids in equilibrium with NaCl brines reported by Chiodini et al. (2001) for 3 m NaCl aqueous fluids. The MRK equations were solved simultaneously, for the equilibration pressure (P) and f_{CO_2}, by fixing the values of f_{H_2O} and temperatures estimated according to Chiodini's model. Notice that the two MRK equations will lead to slightly different pressures but identical CO_2 fugacities[1].

MRK equation of Holloway (1977; 1987)							MRK equation of Kerrick and Jacob (1981)					
date	X_{H_2O}	T (°C)	P (MPa)	f_{H_2O}	f_{CO_2} Chiodini et al. (2001)	f_{CO_2} (this work)	X_{H_2O}	T (°C)	P (MPa)	f_{H_2O}	f_{CO_2} Chiodini et al. (2001)	f_{CO_2} (this work)
190497	0.910	467	166	497	92	49	0.910	467	175	497	92	49
230498	0.843	452	170	436	73	81	0.843	452	174	436	73	81
240698	0.898	452	160	438	66	50	0.898	452	166	438	66	50
141198	0.895	454	161	443	68	52	0.895	454	166	443	68	52
50299	0.901	448	156	422	69	47	0.901	448	162	422	69	47
280799	0.895	445	154	408	67	48.	0.895	445	160	408	67	48.
280899	0.911	445	152	410	66	40	0.911	445	158	410	66	40
250999	0.910	437	147	381	58	38	0.910	437	152	381	58	38
141099	0.907	431	144	360	54	37	0.907	431	148	360	54	37
230498	0.784	436	172	378	67	104	0.784	436	169	378	67	104
240698	0.924	447	151	418	62	34	0.924	447	158	418	62	34
141198	0.887	436	150	376	55	48	0.887	436	154	376	55	48
280799	0.895	439	150	386	63	45	0.895	439	155	386	63	45
P ave			156.4 ± 8.8						161.3 ± 8.3			

[1]. Assuming ideal mixing, the equilibration pressures are slightly higher (of about 5 MPa), but CO_2 fugacities would be unrealistically higher.

Table 3. Summary of calculations for a double convective cell model of the deep hydrothermal system at Somma-Vesuvius. Fluid data are for pure water (Lemmon et al., 2005): η_f, ρ_f and C_f are the average fluid viscosity, the fluid density and the specific heat within the upper cells (*uc*) and the lower cells (*lc*), respectively. They were estimated at 450°C and 40 MPa and 120 MPa (values appropriate for the centers of the convecting cells, Fig. 6).

INPUT PARAMETRS				
UPPER CELLS		LOWER CELLS		
$\eta_{w\,uc}$	3.8×10^{-5}	$\eta_{w\,lc}$	8×10^{-5}	Pa s
$\rho_{w\,uc}$	280	$\rho_{w\,lc}$	650	kg/m^3
ρ_m	2700	ρ_m	3000	kg/m^3
k_{uc}	1×10^{-12}	k_{lc}	1×10^{-15}	m^2
H_{uc}	3	H_{lc}	2.8	km
$C_{w\,uc}$	9.8×10^3	$C_{w\,lc}$	5×10^3	J/kg °C
$R_{a\,(uc)}$	100269	$R_{a\,(lc)}$	107	
CALCULATED PARAMETERS				
Δt_{total} = 3.82 days (half life of ^{222}Rn)				
$v_{f\,(uc)}$	1645	$v_{f\,(lc)}$	1403	m/day
Δt_{uc}	1.82	Δt_{lc}	2	days
ϕ_{uc}	1×10^{-5}	ϕ_{lc}	2.75×10^{-7}	
		ϕ_{bulk}	5.3×10^{-6}	
Δt_{total} = 13.5 days (maximum duration of ^{222}Rn anomalies)				
$v_{f\,(uc)}$	1645	$v_{f\,(lc)}$	240	m/day
Δt_{uc}	1.82	Δt_{lc}	11.68	days
ϕ_{uc}	1×10^{-5}	ϕ_{lc}	1.6×10^{-6}	
		ϕ_{bulk}	6×10^{-6}	

Table 4. Summary of calculations for a double convective cell model of the deep hydrothermal system at Somma-Vesuvius. Fluid density ($\rho_{f\,mix}$) and viscosity ($\eta_{f\,mix}$) were estimated for an aqueous fluid with 2 % of NaCl, at 450°C and 40 MPa and 120 MPa (values appropriate for the centers of the convecting cells, Fig. 6). Thermal expansion of the fluid mixture (2% NaCl): $\alpha_{f\,mix} = 1.963 \times 10^{-3}$ °C^{-1}. Other data are from Table 1. See text for details.

INPUT PARAMETRS				
UPPER CELLS		LOWER CELLS		
$\eta_{f\,mix\ (uc)}$	5.37×10^{-5}	$\eta_{f\,mix\ (lc)}$	5.42×10^{-4}	Pa s
$\rho_{f\,mix\ (uc)}$	315	$\rho_{f\,mix\ (lc)}$	678	kg/m^3
ρ_m	2700	ρ_m	3000	kg/m^3
$C_{f\ mix\ (uc)}$	9.62×10^3	$C_{f\ mix\ (lc)}$	4.92×10^3	J/kg °C
k_{uc}	1×10^{-12}	k_{lc}	1×10^{-15}	m^2
H_{uc}	3	H_{lc}	2.8	km
$R_{a\ (uc)}$	78410	$R_{a\ (lc)}$	162	
CALCULATED PARAMETERS				
Δt_{total} = 3.82 days (half life of ^{222}Rn)				
$v_{f\,mix\ (uc)}$	1315	$v_{f\,mix\ (lc)}$	1819	m/day
Δt_{uc}	2.28	Δt_{lc}	1.54	days
ϕ_{uc}	1×10^{-5}	ϕ_{lc}	2.8×10^{-7}	
		ϕ_{bulk}	5.3×10^{-6}	
Δt_{total} = 13.5 days (duration of ^{222}Rn anomalies)				
$v_{f\,mix\ (uc)}$	1315	$v_{f\,mix\ (lc)}$	250	m/day
Δt_{uc}	2.28	Δt_{lc}	11.21	days
ϕ_{uc}	1×10^{-5}	ϕ_{lc}	2×10^{-6}	
		ϕ_{bulk}	6.15×10^{-6}	